Hindawi
International Journal of Aerospace Engineering
Volume 2020, Article ID 8882343, 19 pages
https://doi.org/10.1155/2020/8882343

Research Article

Combustion Turbulence Flow in Trapped Vortex Combustor with Guide Vane and Blunt Body

Zhuoxiong Zeng, Kaifang Guo, and Xue Gong

College of Power and Mechanical Engineering, Shanghai University of Electric Power, Shanghai 200090, China

Correspondence should be addressed to Zhuoxiong Zeng; zengzhx@163.com

Received 20 April 2020; Revised 1 September 2020; Accepted 12 September 2020; Published 27 September 2020

Academic Editor: Antonio Viviani

Numerical calculation was conducted to obtain the optimum structure parameters of the trapped vortex combustor (TVC) with the guide vane and blunt body. The results show that the optimum structure parameters of the guide vane are $a/H_f = 0.5$, $b/L_i = 0.2$, and $c/L = 0.1$, and the optimum structure parameters of blunt body are $S/L = 0.7$, $L2/L = 0.1$, and $L1/L_i = 0.25$. Then, the influence of different inlet conditions on the combustion turbulence flow was studied. The results show that high inlet temperature and low inlet velocity can effectively reduce total pressure loss; the equivalence ratio has little effect on total pressure loss. The study of unsteady flow shows that double vortices undergo the process of preliminarily forming-breaking down-forming again-being stable gradually.

1. Introduction

The trapped vortex combustor (TVC) [1, 2] was proposed to meet the performance requirements of high temperature rise and low pollution for the modern gas turbine and aircraft engine. This concept combustor attracts more and more attention because of its characteristics of simple structure, small pressure loss, good flame stability, and high combustion efficiency [3–5].

Ezhil and Mishra [6] numerically investigated the reacting flow characteristics of a 2D trapped vortex combustor. The vortex core location shifts with variation in operating condition, and temperature contours at locations downstream of the trailing edge indicate that both cavity flames are merged together for higher primary air velocity cases. Chen and Zhao [7] numerically investigated the effects of guide vanes on the performance of a trapped vortex combustor by three-dimensional steady and unsteady simulations. The results reveal that the introduction of guide vanes significantly changes the cavity vortex structure. Zhu et al. [8] studied a trapped vortex combustor to understand the effects of the angle and location of primary injection on the cavity flow structure with both experimental and numerical methods. Two different flow structures have been found out with different combinations of the inlet angle of the primary injection (θ) and the distance between the primary injection and the bottom wall of the cavity (H). Li et al. [9] conducted an experiment to investigate the effect of strut length on combustion performance of a trapped vortex combustor. The results show that lean blowout (LBO) and combustion efficiency depend upon the strut length to a great extent. Numerical simulations were also performed to explain the experimental results. Sharifzadeh and Afshari [10] carried out a numerical simulation on the flow field in a trapped vortex combustor. The predicted results show that configurations with both air and fuel jets adjacent to the mainstream or adjacent to the cavity inferior wall leads to more homogeneous mixture and a better global fuel distribution. Ezhil and Mishra [11] experimentally characterize the 2D twin cavity TVC in terms of its visible flame length, pollutant emission level, and exit temperature; results reveal that visible flame length value is sensitive to mainstream Reynolds number, primary (cavity) air velocity, and cavity equivalence ratio. And numerical results are also discussed to explain certain intricacies in flow and flame characteristics; numerical studies indicate that shortening of flame length at higher Re cases

is caused due to quenching of flame at the shear layer by the incoming flow. Wu and He [12] designed a trapped vortex combustor with replaceable bluff bodies to experimentally investigate these processes. The combustion process was analyzed theoretically in the viewpoints of relative evaporation time, mixing time, and reaction time. Numerical simulations were also conducted to help analyze the formation and depletion processes of pollutants in TVC. Xie and Zhu [13] designed a modified advanced vortex combustor, which is a kind of TVC, to overcome the incomplete combustion of fuel. The results show that the proposed advanced vortex combustor achieves excellent efficiency, low NOx emissions, a uniform outlet temperature distribution, enhanced outlet velocity, and acceptable total pressure loss. Deng et al. [14] experimentally and numerically studied the flow characteristics of an AVC in a rectangular channel and an annular channel to provide an optimized configuration of an advanced vortex combustor (AVC). Zeng et al. [15] performed numerical calculation to analyze the combustion flow in different advanced vortex combustors; the performance of the advanced vortex combustor with vortex generator principle is obviously better than that without vortex generator. Agarwal et al. [16, 17] combined the guide vane and inclined struts with TVC; results show that it obtained better performance than TVC without the guide vane and inclined struts.

In this paper, based on the structure of TVC and the previous study [16], a trapped vortex combustor with the guide vane and blunt body was proposed. However, the effect of the guide vane and blunt body structure parameters on the combustor is very important. The vortex structures and flow characteristics of TVC are sensitive to the structure parameters of the guide vane and blunt body. Hence, it is necessary to study the structural parameters of TVC to obtain the optimal structural parameters in order to improve the performance of TVC. Simulation on unsteady flow was also performed to analyze the variation of double vortex structure. Moreover, based on the optimal structure, the effect of different inlet conditions on the combustion flow of TVC was studied.

2. Geometric Model, Governing Equations, and Boundary Conditions

2.1. Geometric Model. Figure 1 shows the geometric model of three-dimensional TVC with the guide vane and blunt body. Combustor length is 250 mm, $L_i = 50$ mm is defined as the depth of the combustor inlet, and the guide vane has a thickness of 1 mm. The size of the inlet face is 50 mm × 30 mm. $H_f = 30$ mm is defined as the depth of the cavity, and $L = 36$ mm is the length of the cavity. Position parameters (a, b, c) of the guide vane and structure parameters (S, $L2$, $L1$) of the blunt body are marked in Figure 1. In this paper, a is the length of the guide vane inside the cavity, b is defined as the distance from the guide vane to the cavity leading edge, and c is the distance from the guide vane to the cavity fore wall. S is the distance from the blunt body to the cavity fore wall, $L2$ is defined as the length of the blunt body, and $L1$ is the height of the blunt body. Structure parameters of the guide vane and blunt body are listed in Table 1.

2.2. Governing Equations and Boundary Conditions. The governing equations can be summarized as follows.

The continuity equation is given as

$$\frac{\partial \rho}{\partial t} + \frac{\partial}{\partial x_j}\left(\rho \bar{u}_j\right) = 0. \tag{1}$$

The momentum equation is given as

$$\frac{\partial}{\partial t}\left(\rho \bar{u}_i\right) + \frac{\partial}{\partial x_j}\left(\rho \bar{u}_i \bar{u}_j\right) = \frac{\partial}{\partial x_j}\left[\mu\left(\frac{\partial \bar{u}_i}{\partial x_j} + \frac{\partial \bar{u}_j}{\partial x_i}\right)\right] - \frac{\partial \bar{p}}{\partial x_i} + \rho f_i. \tag{2}$$

The energy equation is given as

$$\frac{\partial \rho c_p \bar{T}}{\partial t} + \frac{\partial}{\partial x_j}\left(\rho c_p \bar{T} \bar{u}_j\right) = \frac{\partial}{\partial x_j}\left(\lambda \frac{\partial \bar{T}}{\partial x_j}\right) + \bar{w}_s Q_s. \tag{3}$$

The species equation is given as

$$\frac{\partial \rho \bar{Y}_s}{\partial t} + \frac{\partial}{\partial x_j}\left(\rho \bar{u}_j \bar{Y}_s\right) = \frac{\partial}{\partial x_j}\left(\frac{\mu}{S_C}\frac{\partial \bar{Y}_s}{\partial x_j}\right) - \bar{w}_s. \tag{4}$$

The turbulence kinetic energy equation and the turbulence kinetic energy dissipation equation [18] are listed as follows:

$$\frac{\partial(\rho k)}{\partial t} + \frac{\partial\left(\rho k \bar{u}_j\right)}{\partial x_j} = \frac{\partial}{\partial x_i}\left[\left(\mu + \frac{\mu_t}{\sigma_k}\right)\frac{\partial k}{\partial x_i}\right] + \mu_t \frac{\partial \bar{u}_j}{\partial x_i}\left(\frac{\partial \bar{u}_i}{\partial x_j} + \frac{\partial \bar{u}_j}{\partial x_i}\right) - \rho\varepsilon, \tag{5}$$

$$\frac{\partial(\rho\varepsilon)}{\partial t} + \frac{\partial\left(\rho\varepsilon \bar{u}_j\right)}{\partial x_j} = \frac{\partial}{\partial x_i}\left[\left(\mu + \frac{\mu_t}{\sigma_\varepsilon}\right)\frac{\partial \varepsilon}{\partial x_i}\right] + c_1 \rho S_\varepsilon - c_2 \rho \frac{\varepsilon^2}{k + \sqrt{\nu\varepsilon}}. \tag{6}$$

The eddy dissipation model is given as [19]

$$\bar{w}_s = -A_{\mathrm{EBU}} \bar{\rho} \frac{\varepsilon}{k} \min\left\{\overline{Y_{CH_4}}, \frac{\overline{Y_{O_2}}}{\beta}, B_{\mathrm{EBU}} \frac{\overline{Y_P}}{1+\beta}\right\}. \tag{7}$$

The method of pressure and velocity coupling is SIMPLE [20]; second-order central difference scheme and second-order upwind difference scheme are used for the diffusion terms and the convective terms individually. To obtain a grid independent solution, the computation domain is meshed with 1351 962 mixed (hybrid) cells.

The mainstream inlet velocity is 50 m/s, inlet temperature is 300 K, and equivalence ratio is 0.6. Gaseous methane fuel (CH_4) is premixed at the inlet. Outlet pressure boundary and convection combustor wall boundary are adopted. For the blunt body and guide vane, the coupled convective heat transfer boundary is adopted. At the wall, no-slip condition is used.

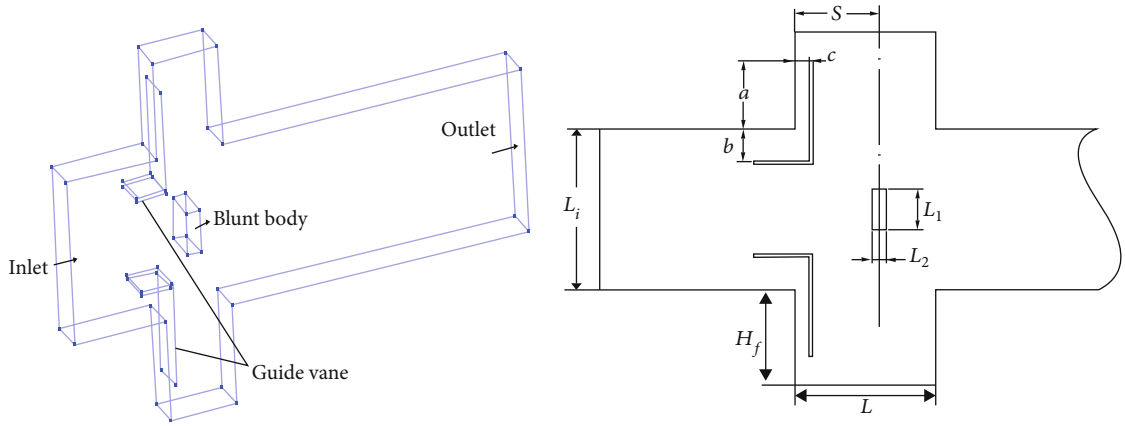

Figure 1: The geometric model of TVC.

Table 1: Structure parameters of the guide vane and blunt body.

S/L		0.5	0.6	0.7	
$L2/L$		0.1	0.2	0.3	
$L1/L_i$	0.15	0.2	0.25	0.3	0.35
a/H_f	0.5	0.6	0.7	0.8	0.9
b/L_i		0.1	0.2	0.3	
c/L		0.05	0.1	0.15	

3. Results and Discussions

The comparison between experiment [17] and calculation results is shown in Figure 2. For most comparison of experiment and simulation, the error is relatively small as a whole. Thus, the models and boundary conditions in this paper are acceptable.

3.1. Optimum Structure of the Blunt Body. The total pressure loss is

$$\delta^* = \frac{P_1^* - P_2^*}{P_1^*}, \tag{8}$$

where $P_1{}^*$ is the inlet total pressure and $P_2{}^*$ is the outlet total pressure.

The combustion efficiency is

$$\eta = 1 - \frac{\sum \mathrm{EI_x LHV_x}}{1000 \mathrm{LHV_f}}, \tag{9}$$

where EI (g/kg) is the pollutant emission index, LHV (kJ/kg) is the low calorific value, subscript x is various pollutant emissions, and subscript f is fuel.

Figure 3 shows the influence of S, $L1$, and $L2$ on total pressure loss. It can be found that with the increase of S, total pressure loss decreases. The height $L1$ has the greatest influence on total pressure loss; the larger $L1$ is, the greater the total pressure loss. The smaller the length $L2$ is, the smaller the total pressure loss.

Total pressure loss is mainly caused by the obstruction of the guide vane and blunt body, as well as the double vortices in the cavity and in the backflow region behind the blunt body. As shown in Figure 3(a), when $S/L = 0.5$, in the process of combustion, due to the thermal expansion of combustion products, the surrounding gas is squeezed to flow toward the mainstream. The obstruction of the blunt body decelerates the gas in the windward part of the blunt body, and the gas around the blunt body accelerates. The closer the blunt body is to the guide vane, the greater the effect of the accelerated gas on the secondary vortex in the cavity. The larger $L2$ is, the greater total pressure loss is, and total pressure loss increases with the increase of $L1$. The length $L2$ is parallel to the mainstream direction, which does not have a great impact on the gas flow. However, with the increase of $L2$, the time of gas flowing on the blunt body surface becomes longer, and the effect of turbulent viscosity becomes stronger, so total pressure loss increases to some extent. The height $L1$ is related to the blocking degree of the main channel. The larger $L1$ is, the greater the blocking degree is. After the gas flows through the blunt body, due to the influence of the reverse pressure gradient formed behind the blunt body, the larger the backflow region appears behind the blunt body, so the increase of $L1$ is bound to increase total pressure loss. When $S/L = 0.5$, the structure with the smallest total pressure loss is $L1/L_i = 0.15$, $L2/L = 0.1$, and total pressure loss is 5.92%.

As shown in Figures 3(b) and 3(c), with the increase of S, the blunt body is more far away from the guide vane; the influence of the main flow on the secondary vortex in the cavity decreases, so total pressure loss decreases. When $S/L = 0.7$, the influence of blunt body length $L2$ on total pressure loss becomes smaller. When $S/L = 0.6$ and $S/L = 0.7$, the minimum total pressure loss is 5.85% and 5.80%, respectively, and the corresponding structure is also $L1/L_i = 0.15$ and $L2/L = 0.1$.

Figure 4 shows the flow field distributions under different blunt body parameters. The main flow is divided into two parts by the guide vane, the double vortex structure can be formed in the cavity, and the vortex structure is basically similar. The main vortex is formed by the gas from the guide

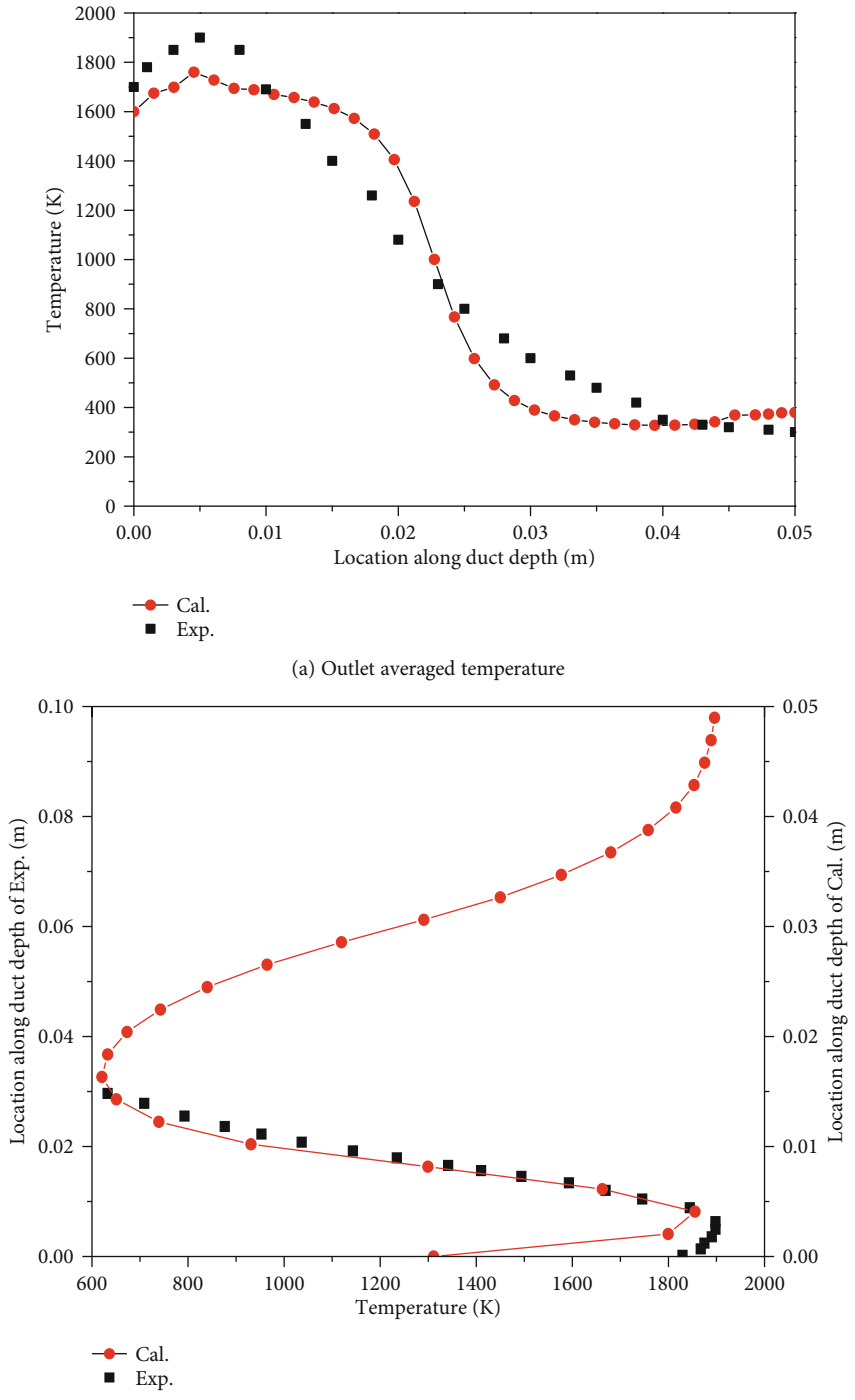

(a) Outlet averaged temperature

(b) Outlet radial temperature distribution

Figure 2: Comparison of experiment and calculation.

vane into the cavity; its core is close to the cavity rear wall. There is a secondary vortex between the main flow and the main vortex. The secondary vortex core is close to the cavity front wall, and the streamline between the two flows is from the main stream to the cavity, which is conducive to the mixing of fuel and gas.

As shown in Figure 4(a), the flow field changes along with $L1$ ($S/L = 0.7$, $L2/L = 0.1$). It can be seen that as the height $L1$ increases, the backflow region behind the blunt body has obvious changes; its size is getting bigger and bigger. The bigger backflow region means that it has greater ability to absorb the unreacted gas for reaction. A stable double vortex structure can be formed in the cavity. However, the higher the blunt body, the greater the obstruction to the main flow and the bigger the gas velocity passing around the blunt body. Therefore, the influence of the main flow on the double vortex structure in the cavity will also increase, which shows that with the increase of $L1$, the vortex cores of the main vortex

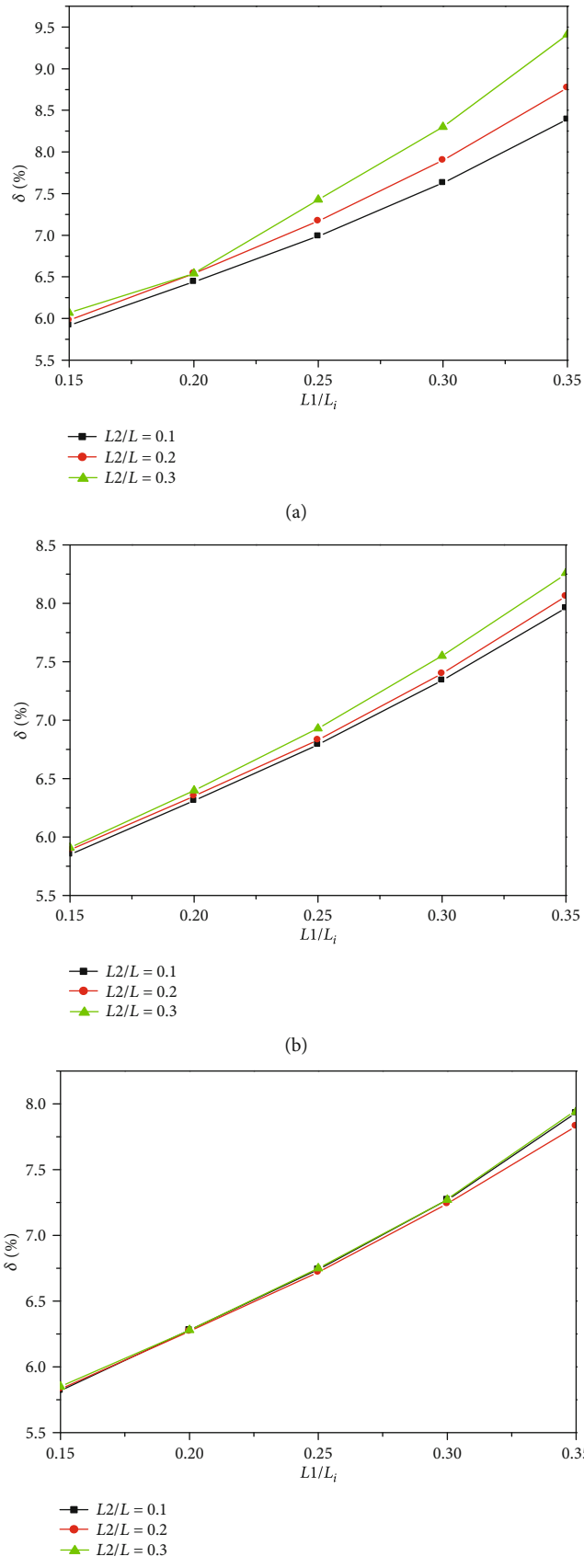

Figure 3: Total pressure loss under different blunt bodies. (a) $S/L = 0.5$, (b) $S/L = 0.6$, and (c) $S/L = 0.7$.

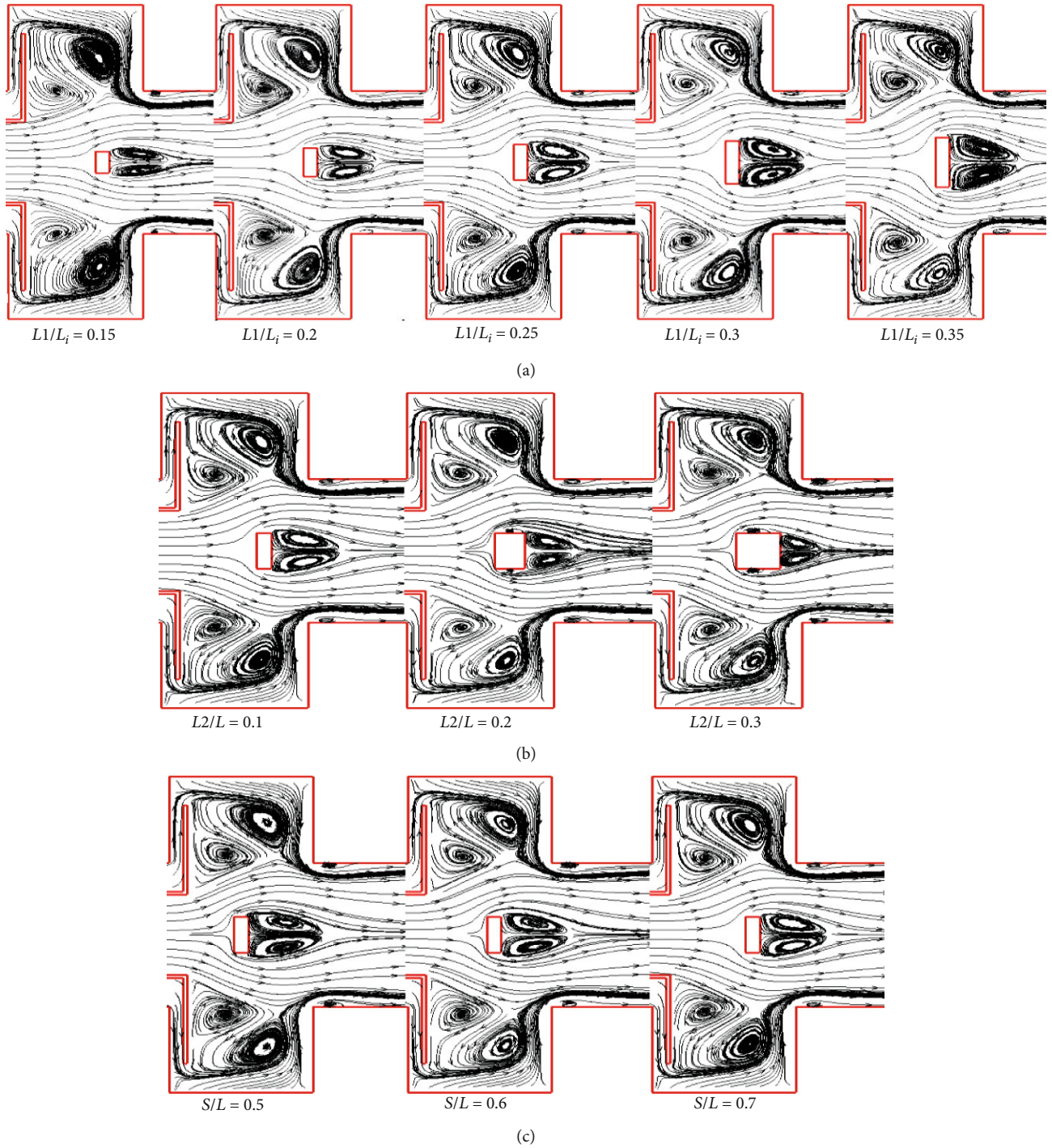

Figure 4: Flow field under different blunt bodies. (a) Different $L1$, (b) different $L2$, and (c) different S.

and the secondary vortex move towards the cavity bottom, and the size of the secondary vortex changes little, while the size of the main vortex decreases.

The flow field distribution under different $L2$ ($L1/L_i = 0.25$, $S/L = 0.7$) is shown in Figure 4(b). It can be seen that there are still relatively stable double vortices in the cavity, and the vortex core and the vortex region are basically unchanged, which indicates that the change of the length $L2$ has little effect on the structure of the double vortices in the cavity. With the increase of $L2$, the backflow area behind the blunt body decreases gradually, which is not conductive to absorbing unreacted gas to participate in the combustion. In addition, with the increase of $L2$, when the gas flows through its surface, the influence of the surface on its

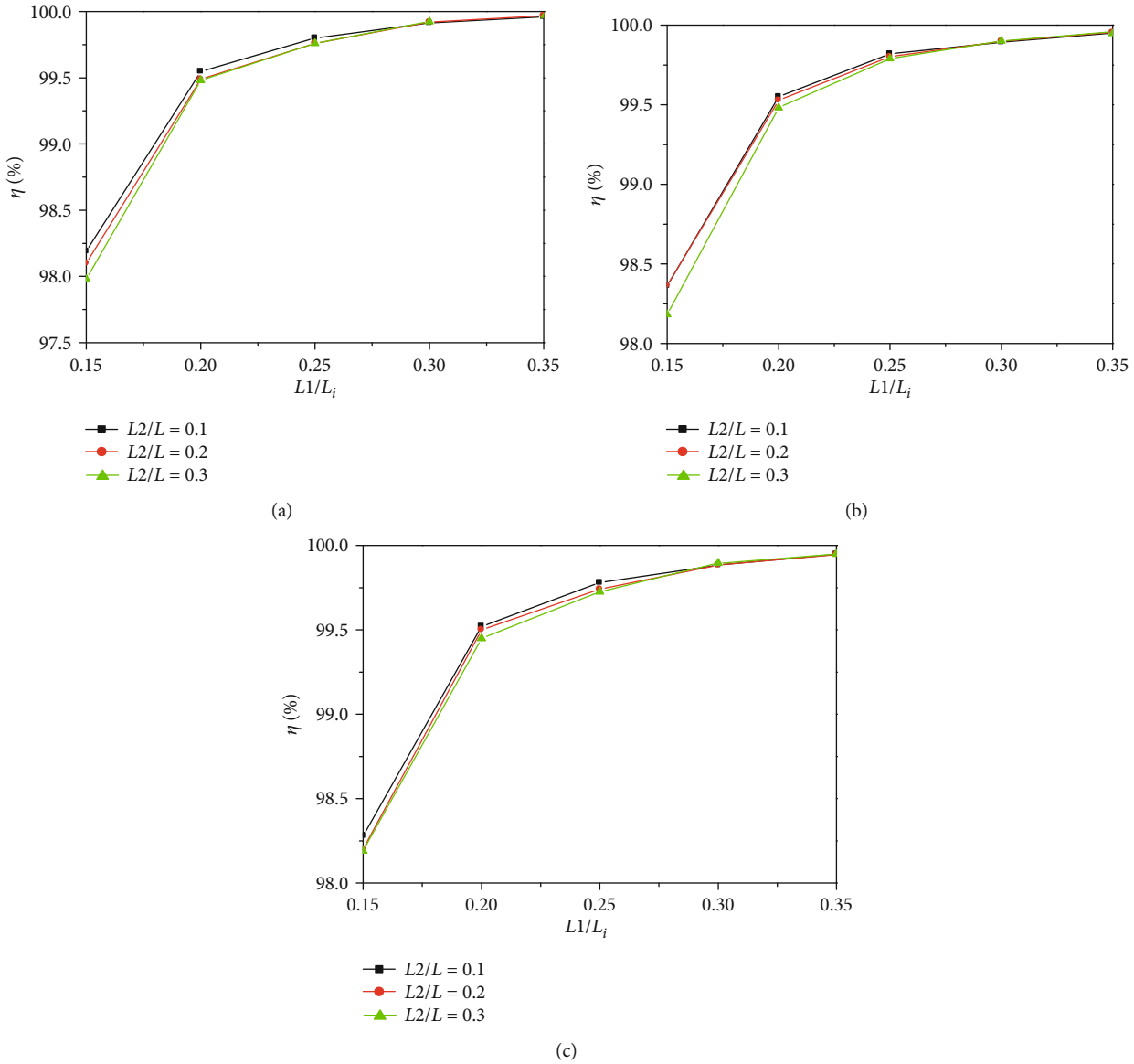

Figure 5: Combustion efficiency under different blunt bodies. (a) $S/L = 0.5$, (b) $S/L = 0.6$, and (c) $S/L = 0.7$.

viscosity is also increased, and the gas velocity near the wall is reduced, which forms a small vortex on the blunt body surface. When $L2/L = 0.3$, the vortex is very obvious.

The flow field distribution under different S is shown in Figure 4(c). With the change of S, the double vortices in the cavity and in the backflow region behind the blunt body do not change much, which shows that the change of blunt body position has little effect on the flow field. With the increase of S, the blunt body is more far away from the guide vane, the main flow reduces the extrusion degree of the secondary vortex in the cavity, and the secondary vortex core moves to the main flow, but the moving distance is very small.

Figure 5 shows the influence of S, $L1$, and $L2$ on combustion efficiency. It can be seen that the influence of S and $L2$ is very small, the main influence factor is the height $L1$, and combustion efficiency increases with the increase of $L1$. Because the larger $L1$ is, the greater the backflow region behind the blunt body is, the more unreacted gas can be sucked for combustion reaction, and the fuel combustion is more complete.

Combined with the above analysis of total pressure loss and the change of vortex, the smaller $L2$ and the larger S, the smaller total pressure loss is and the better the double vortices in the cavity and the backflow region behind the blunt body. Considering all aspects of performance, the better blunt body structure is chosen as $L1/L_i = 0.25$, $L2/L = 0.1$, and $S/L = 0.7$.

3.2. Optimum Structure of the Guide Vane. Figure 6 shows the influence of distance a, b, and c on total pressure loss under different c/L, b/L_i, and a/H_f.

It can be seen that with the increase of distance c, total pressure loss decreases, but the degree of reduction is very small. When the main stream flows through the guide vane,

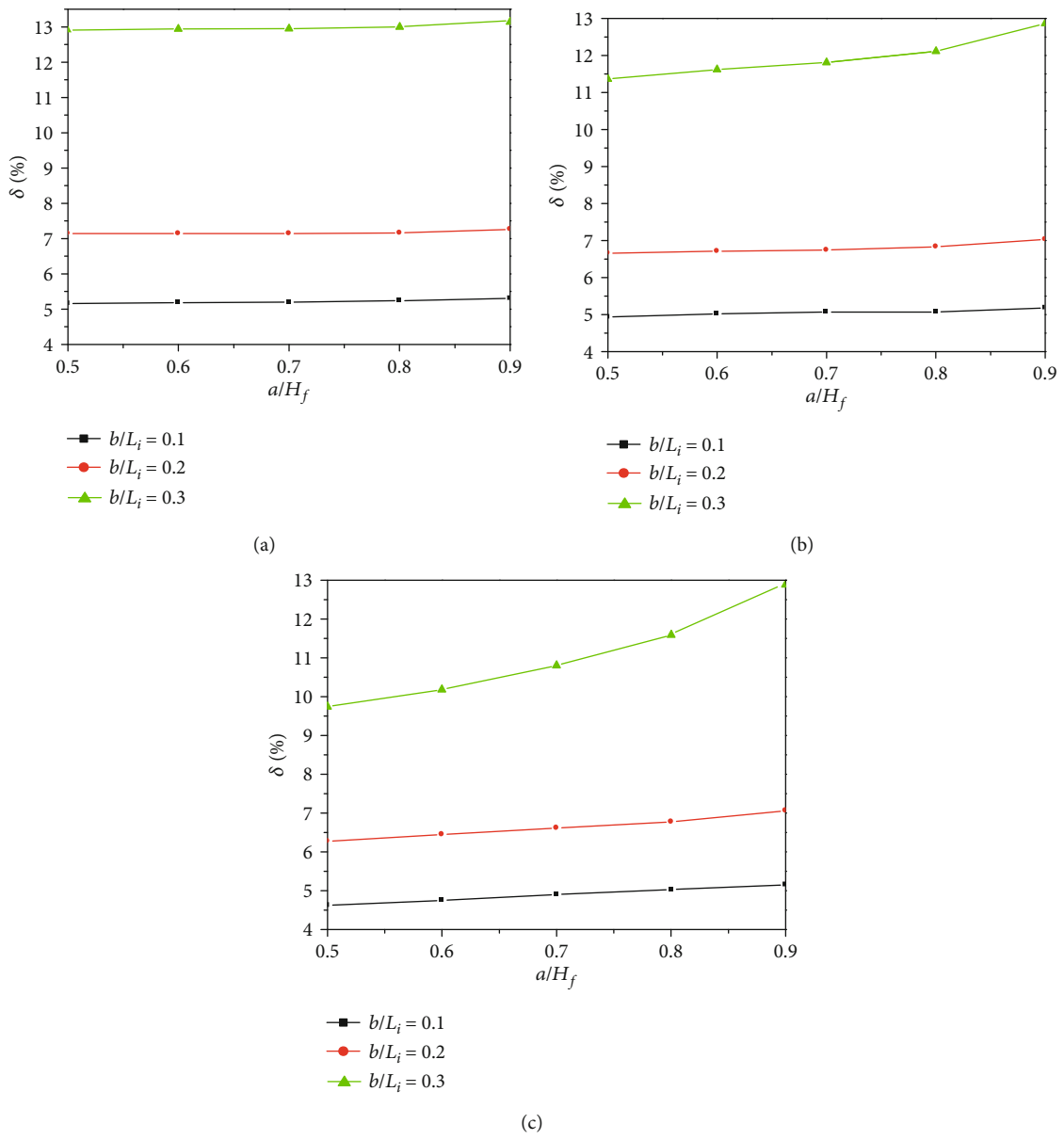

Figure 6: Total pressure loss under different guide vanes. (a) $c/L = 0.05$, (b) $c/L = 0.1$, and (c) $c/L = 0.15$.

part of the gas enters the cavity from the channel between the guide vane and the cavity front wall. When c increases, the channel area also increases, which decreases the gas velocity relatively. Meanwhile, because the guide vane moves to the cavity rear wall, the vortex range in the cavity also decreases, so total pressure loss decreases. In most cases, the change of distance a has little effect on total pressure loss. When $c/L = 0.15$, the change is obvious. The greater the distance a, the larger the range of the main vortex in the cavity. In particular, when $b/L_i = 0.3$, more gas flows toward the cavity, which makes the change more serious, so total pressure loss increases with the increase of a.

Distance b has the greatest influence on total pressure loss; the larger the distance b is, the greater total pressure loss is. When $b/L_i = 0.3$, total pressure loss is more than 10%. This is because the larger the distance b, the narrower the main flow channel area, the larger the double vortex range in the cavity, and the more disordered the main flow between the guide vane and the blunt body. With the increase of b, more main flow enters the channel between the guide vane and the cavity front wall, which increases the gas velocity in the channel, and the flow in the trapped vortex region is more disordered, so total pressure loss changes obviously. In addition, when $b/L_i = 0.1$, the maximum total pressure loss is 5.3%, and the minimum is 4.62%. When $b/L_i = 0.2$, the maximum total pressure loss is 7.26%, and the minimum is 6.27%.

Figure 7 shows the flow field distributions under different guide vanes. The main stream is divided into two streams by

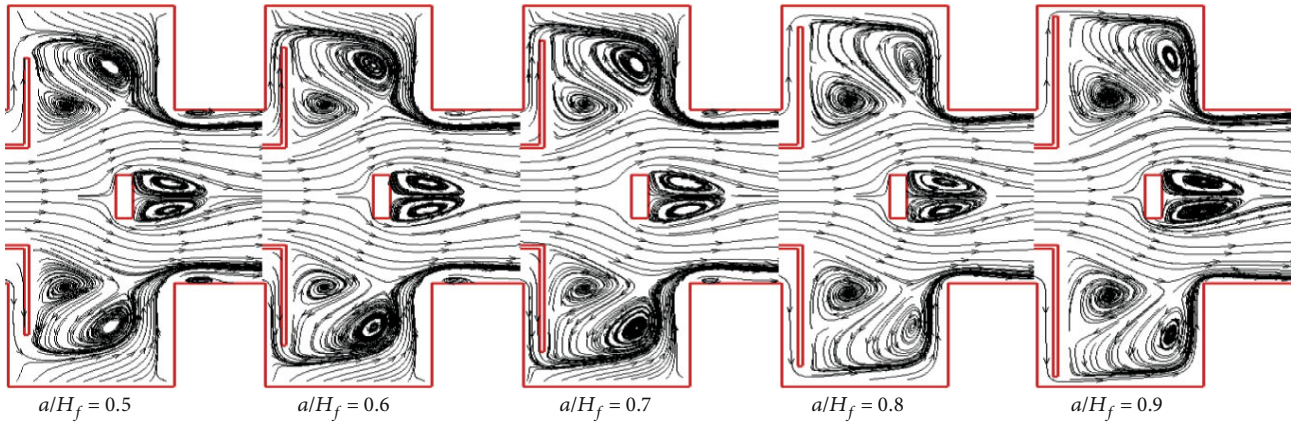

(a)

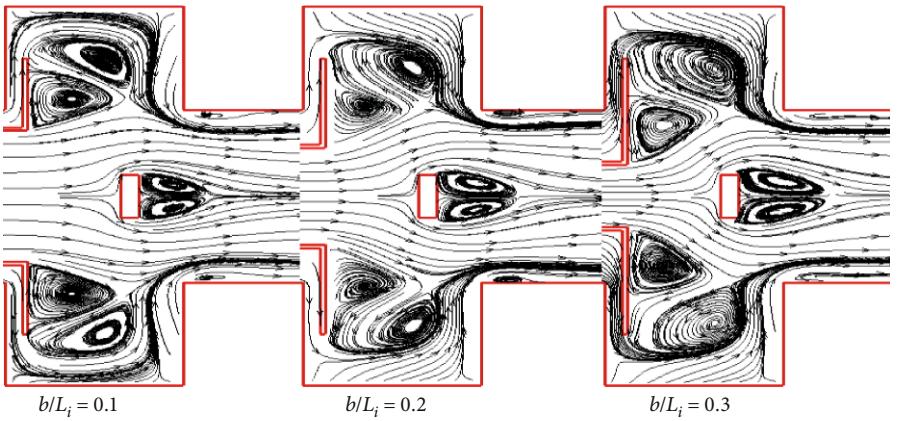

(b)

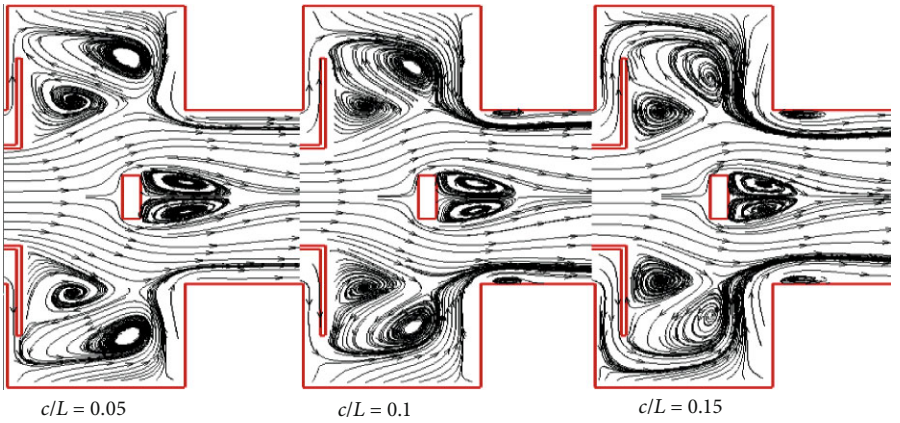

(c)

Figure 7: Flow field under different guide vanes. (a) Different a, (b) different b, and (c) different c.

the guide vane, which can form a double vortex structure in the cavity. And a backflow region behind the blunt body is also formed.

Figure 7(a) reveals the flow field distribution under different distance a. It can be seen that the change of a mainly affects the gas flow in the cavity and does not affect the mainstream; there is basically no change in the backflow region behind the blunt body. With the increase of a, the range of the secondary vortex in the cavity increases, the main vortex gradually develops until it fills the whole cavity, and the vortex core moves to the cavity rear wall. The reason is that after increasing a, the gas entrance from the guide vane to the cavity decreases; especially when $a/H_f = 0.9$, the gas into the cavity closes to the cavity bottom, which makes the main vortex develop near the cavity bottom. With the decrease of the entrance, the velocity of the gas flowing out from the guide vane

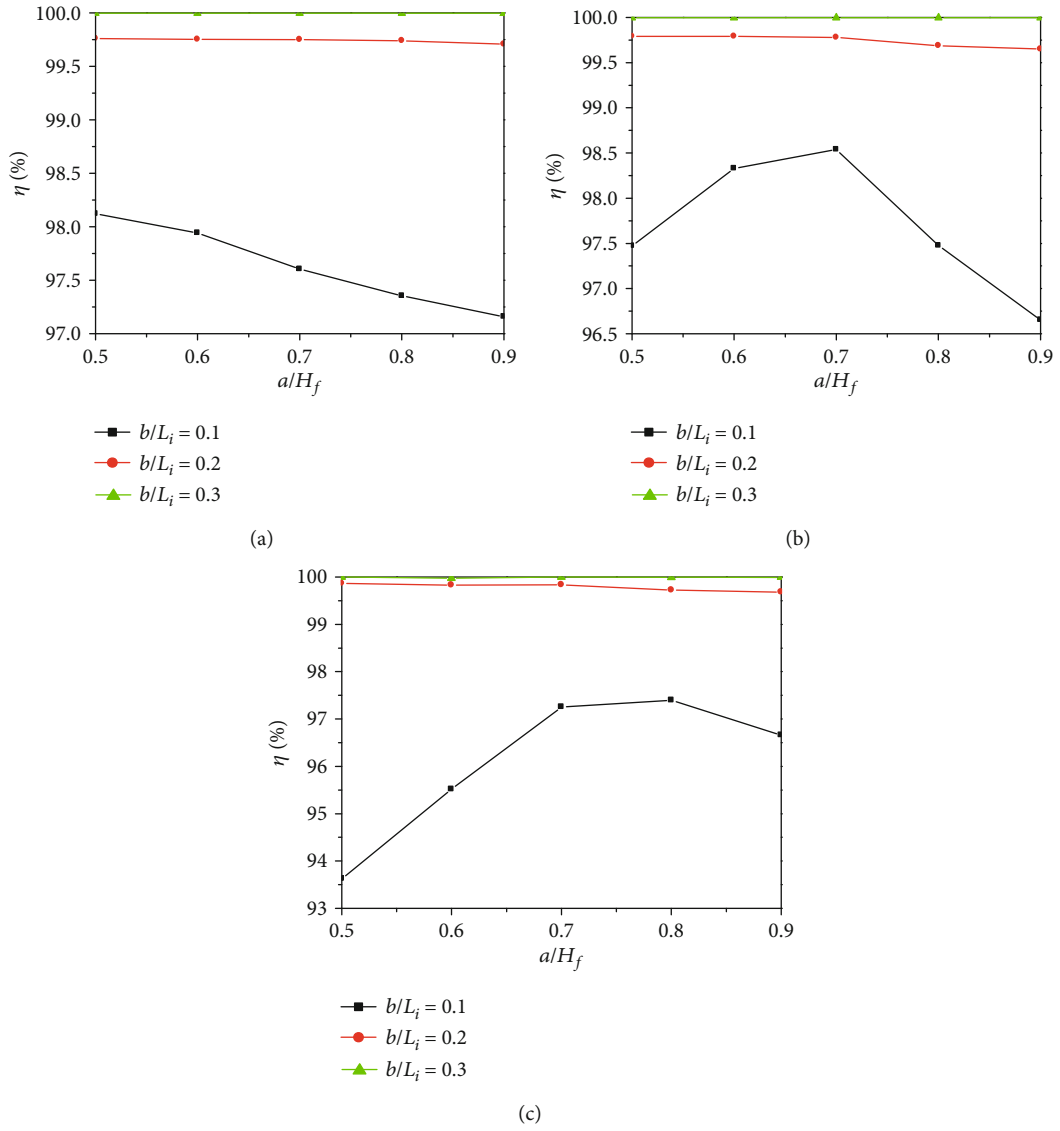

Figure 8: Combustion efficiency under different guide vanes. (a) $c/L = 0.05$, (b) $c/L = 0.1$, and (c) $c/L = 0.15$.

increases, so the main vortex core gradually approaches the cavity rear wall; the range of the secondary vortex also increases.

Figure 7(b) is the flow field distribution under different distance b. The increase of b decreases the main flow channel area correspondingly, and the velocity of main flow gas around the blunt body turns larger, which widens the backflow area behind the blunt body. In the cavity, when $b/L_i = 0.1$, there is less gas flowing into the cavity, so the squeezing effect of the secondary vortex on the main vortex is more obvious, the range of the secondary vortex becomes larger, and the development of the main vortex is not relatively full. When $b/L_i = 0.3$, because the formation of the secondary vortex is related with the guide vane, the secondary vortex core is far away from the cavity with the increase of b, and the main vortex develops more fully with the increase of the gas mass flowing into the cavity.

Figure 7(c) shows the flow field distribution under different distance c. It can be seen that as the distance c increases, the height of the backflow region behind the blunt body does not change nearly, but the length decreases. In the cavity, when $c/L = 0.05$, the gas velocity increases due to the smaller channel area, the main vortex core is close to the cavity rear wall, the secondary vortex is not full, and it shows spiral distribution. With the increase of c, the velocity of the gas entering the cavity decreases, the main vortex core moves to the cavity middle, the squeezing effect of the guide vane on the double vortices increases, and the range of the double vortices also decreases.

Figure 8 shows the influence of distance a, b, and c on combustion efficiency. When $b/L_i = 0.1$, combustion efficiency is relatively low, and the lowest value is about 93.63%. This is because there are a few fuels entering the cavity, and more fuels are not fully reacted in the mainstream, which reduces combustion efficiency. With the increase of b, the range of the double vortex structure in the cavity becomes larger, the range of the backflow region behind the blunt

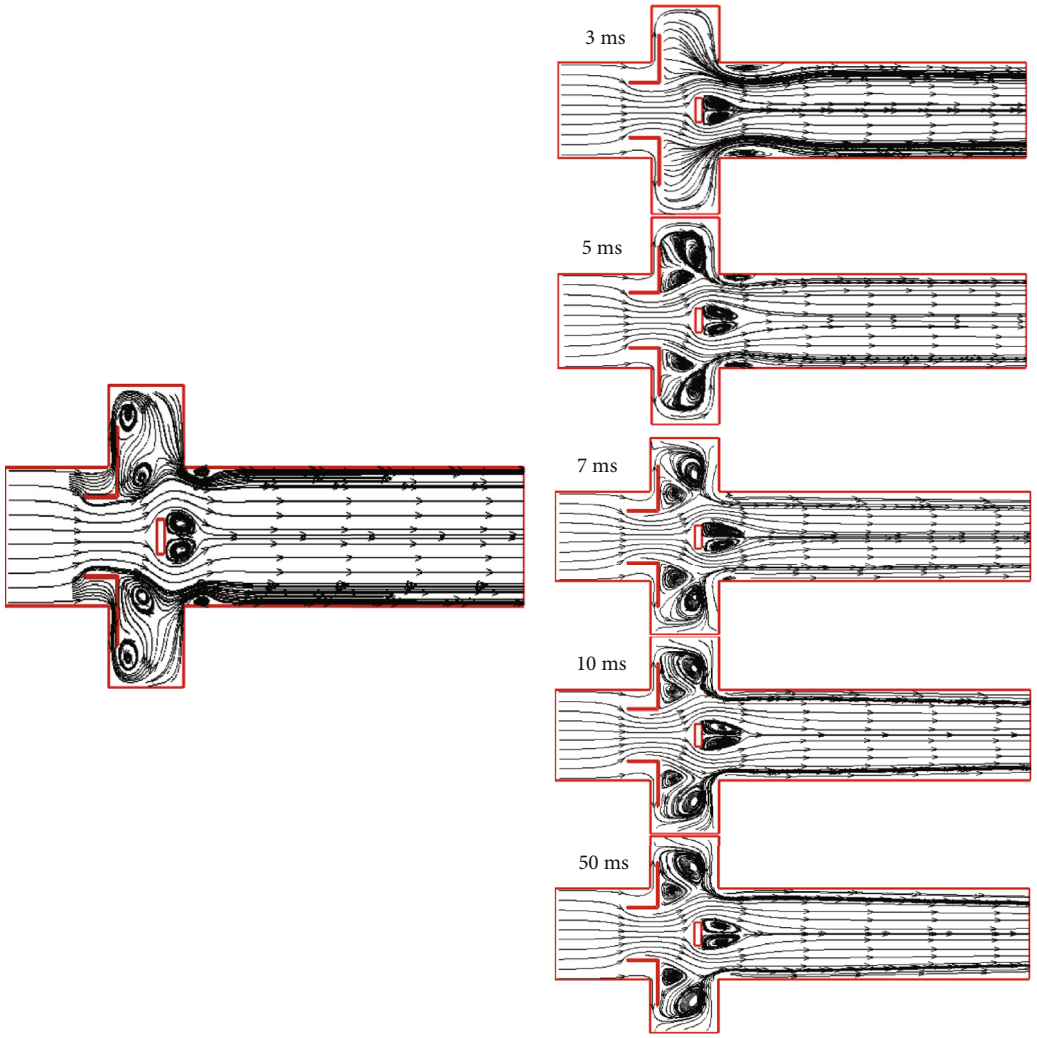

Figure 9: (a) Flow field at 1 ms. (b) Flow field at different times.

body is also larger, and combustion efficiency increases significantly. When $b/L_i = 0.2$ and $b/L_i = 0.3$, combustion efficiency exceeds 99.7%; it varies little regardless of the change of a and c.

According to the above analysis, combustion efficiency is very high when $b/L_i = 0.3$, but total pressure loss is more than 10%. Total pressure loss is better when $b/L_i = 0.1$, but combustion efficiency is lower, so the case of $b/L_i = 0.2$ is the best. For the parameters a and c, the larger the distance a is, the greater total pressure loss is, and the smaller combustion efficiency is. However, when $c/L = 0.1$, the double vortex structure is the most stable, and the range of the backflow region behind the blunt body is also moderate, so the optical guide vane structure is $a/H_f = 0.5$, $b/L_i = 0.2$, and $c/L = 0.1$.

3.3. Unsteady Flow. To show the evolvement and development of the dual vortex, unsteady simulation has been conducted. Figures 9 and 10, respectively, show the flow field and temperature distribution in the combustor at different times. Time step is set to 1.0×10^{-5} s.

From Figure 9(a), at 1 ms, there exists a double vortex structure; the primary vortex core closes to the cavity fore wall. When the mainstream passes over the blunt body, the accelerated mainstream squeezes the secondary vortex behind the guide vane, and the secondary vortex core moves to the inside of the cavity. Because of the effect of inverse gradient pressure formed in the blunt body rear, two symmetric vortices appear behind the blunt body; fuel can be sucked for combustion.

It can be seen from Figure 9(b) that there is no periodic change of vortex shedding and generation in the backflow region behind the blunt body. This is due to the gas high temperature caused by the combustion heat release; there is a strict boundary and a large temperature gradient between the backflow region behind the blunt body and the surrounding gas. The high temperature increases the gas viscosity, and the retardation effect of the blunt body wall on the flame increases, which slows down the flow near the wall. The flow velocity attenuation in the turbulent boundary layer reduces the flame velocity, so the vortex is not easy to shed. In addition, the combustion process is a turbulent process, it has

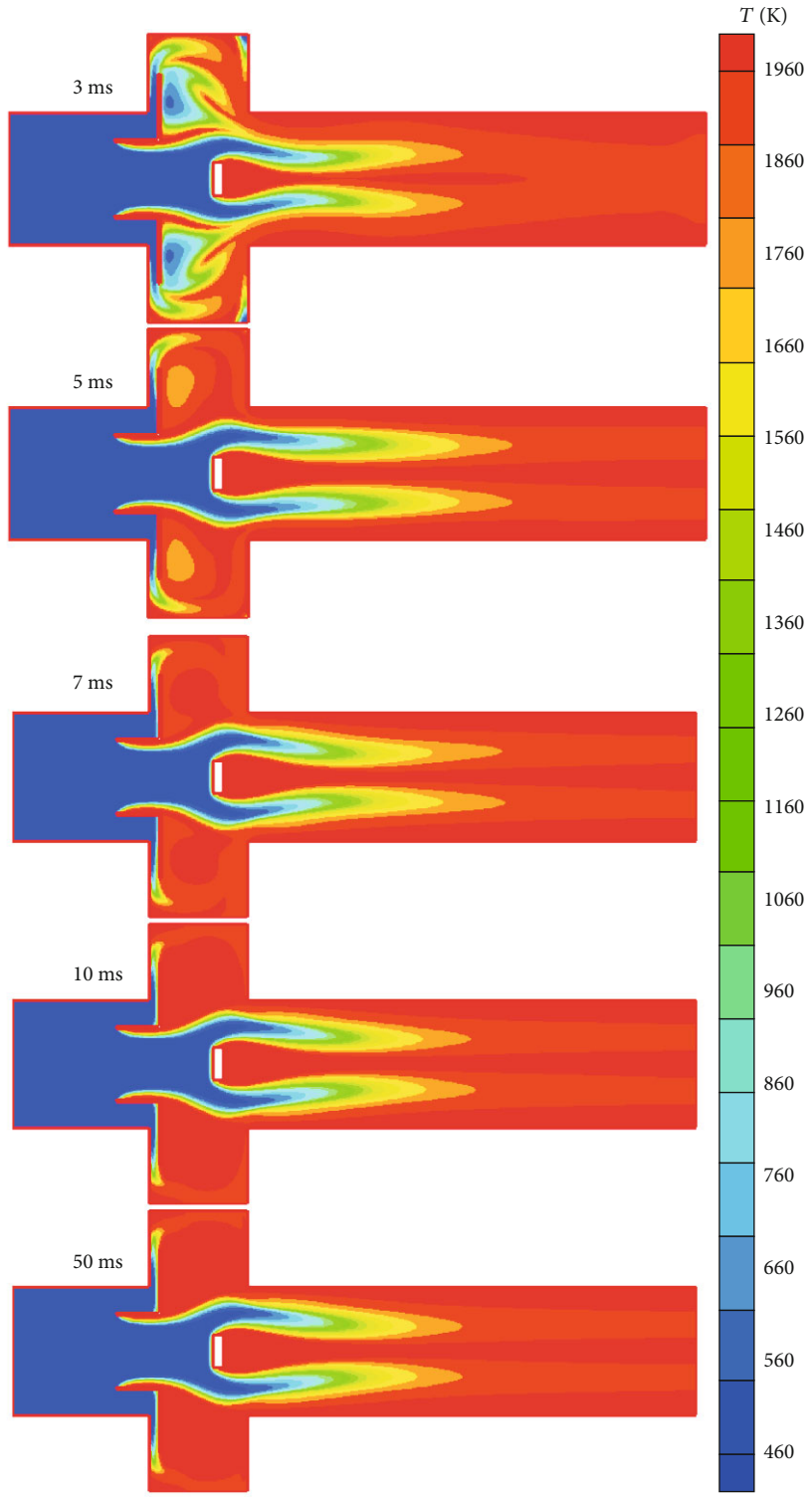

Figure 10: Temperature distribution at different times.

strong dissipation and diffusion; even if there is vortex shedding, it quickly mixes with the surrounding gas and disappears.

At 3 ms, there are no double vortices in the cavity. When the main gas passes by the blunt body, its velocity increases, and when it mixes with the gas flowing out of the cavity, a larger vortex is formed near the cavity rear wall. At 5 ms, the secondary vortex forms again in the cavity; it is more affected by the main flow due to the larger velocity of the main flow. Its vortex core is far away from the guide vane

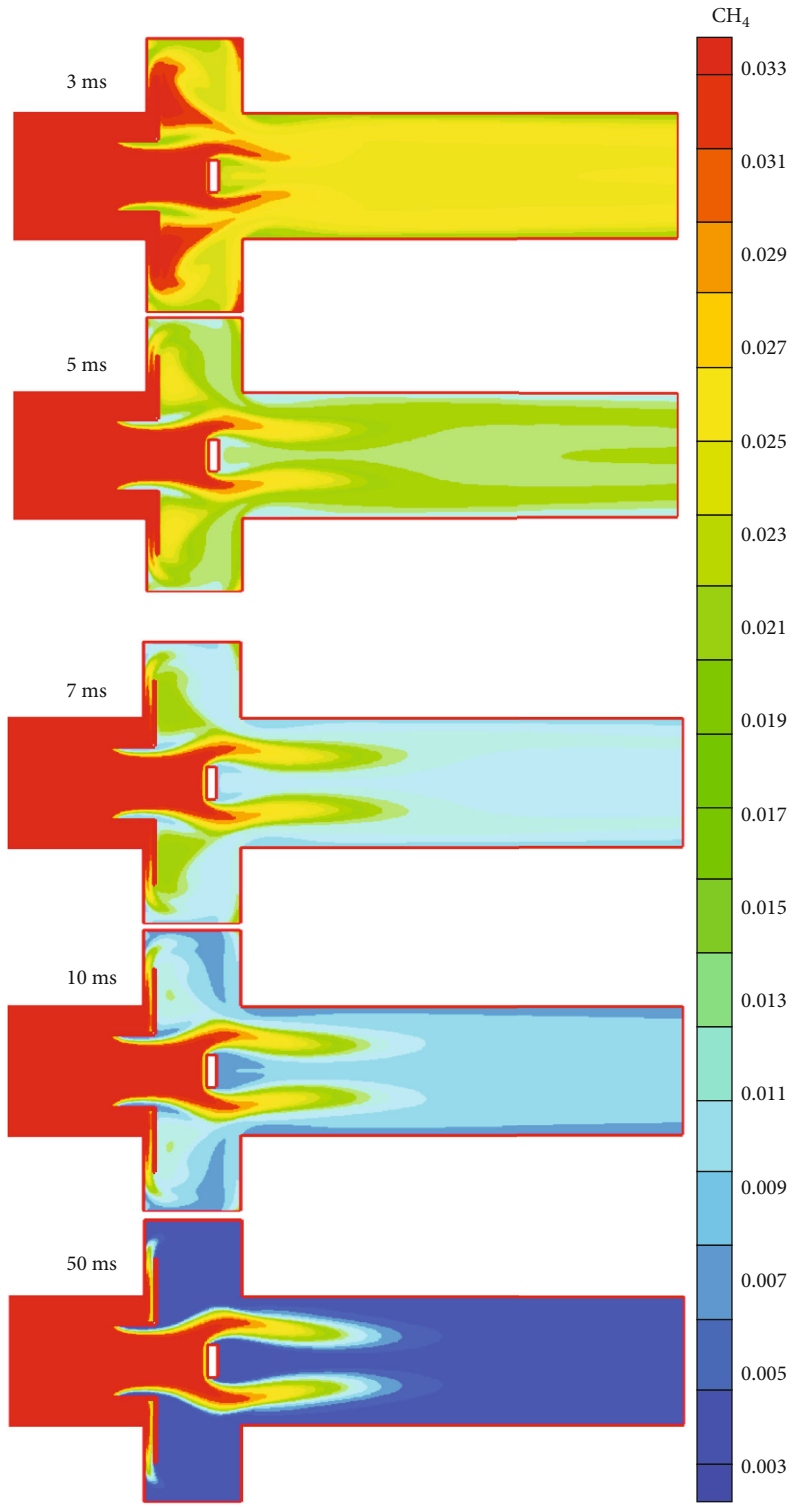

Figure 11: CH_4 mass fraction at different times.

and very close to the main vortex core. The size of the backflow region behind the blunt body remains same nearly, and the vortex size near the cavity rear wall decreases.

From 5 ms to 10 ms, the flow field changes continuously. The double vortex structure in the cavity is more stable, the main vortex turns larger as the reaction proceeds, the vortex core position is basically unchanged, the secondary vortex does not disappear with the change of the main vortex, and the vortex core is gradually close to the guide vane. The range of vortex near the cavity rear wall decreases gradually until it disappears. The height of the backflow region is nearly the same, and the length (parallel to the main flow direction) is

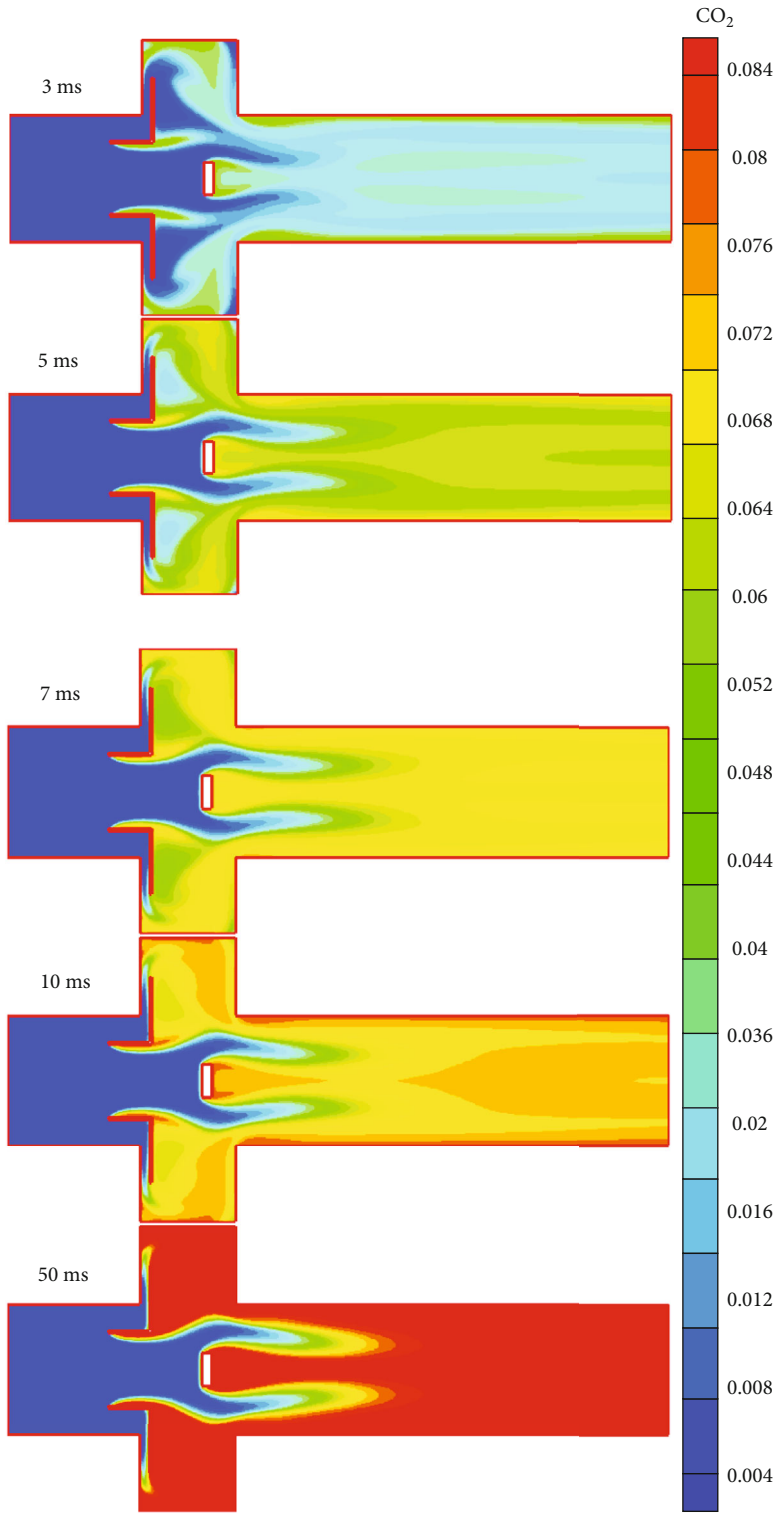

Figure 12: CO_2 mass fraction at different times.

Table 2: Calculation conditions.

Equivalence ratio Φ	0.6	0.8	1.0	1.2	1.4
Inlet velocity V (m/s)	10	20	30	40	50
Inlet temperature T (K)	300	400	500	600	700

increased. When the combustion reaction reaches 50 ms, the flow distribution is basically the same, so the flow field is considered to be stable. The main vortex core in the cavity is closer to the cavity bottom, while the range of the secondary vortex becomes larger. The main vortex is more stable as the ignition source. The vortex near the cavity rear wall

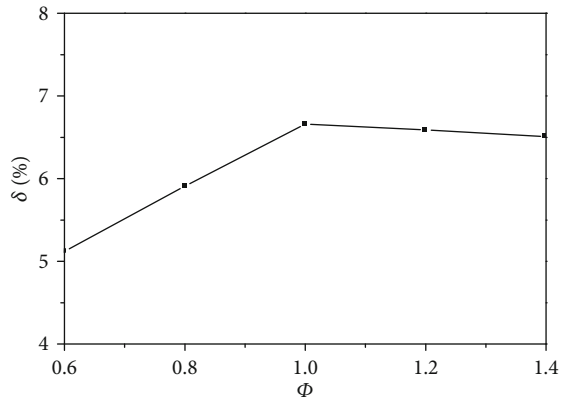

Figure 13: Total pressure loss under different Φ.

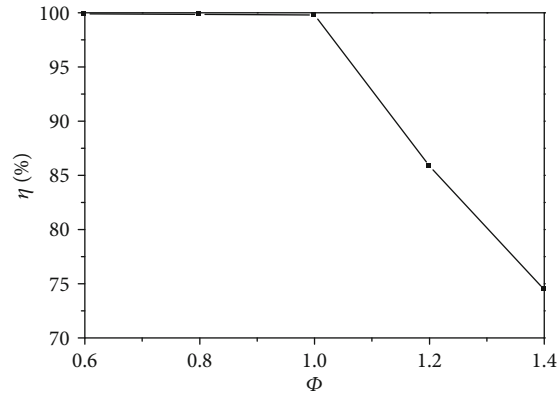

Figure 14: Combustion efficiency under different Φ.

disappears basically, which can avoid unnecessary total pressure loss.

From Figure 10, with the reaction going on, the temperature in the cavity increases gradually; the maximum temperature reaches to about 1900 K. Two streams with low-temperature mixture flowing to the blunt body rear are consumed gradually. There is a small transition region between the low-temperature region and the high-temperature region, and the temperature increases gradually, which indicates that the unreacted gas temperature increases under the influence of the high-temperature products, which can promote the combustion reaction in turn.

Figures 11 and 12, respectively, show the mass fraction distribution of methane and carbon dioxide at different times. Their distributions are just opposite, that is, the region with high methane content is the region with low carbon dioxide content.

It can be seen from Figure 11 that at different times, the methane distributes mainly at the inlet. The cavity and the backflow region behind the blunt body are the main regions of combustion reaction. With the reaction going on, the methane content in these two regions is bound to be smaller and smaller. When the gas flows to the combustor rear part, a lot of oxygen is consumed in combustion, and a lot of carbon is generated; the mass fraction of methane also decreases.

It can be seen from Figure 12 that the distribution of carbon dioxide mass fraction is mainly distributed in the cavity and in the combustor downstream. Due to the existence of the blunt body, the incompletely reactive mixture in the mainstream is sucked into the backflow region behind the blunt body for combustion, so more carbon dioxide is also generated behind the blunt body. At 50 ms, carbon dioxide fills the entire cavity and the combustor rear part; the fuel utilization efficiency is improved.

3.4. The Effect of Inlet Condition on the Combustion Flow of TVC. Different inlet conditions have great influence on the combustion flow; the effect of equivalence ratio Φ, inlet velocity V, and inlet temperature T on the combustion flow field of TVC is discussed.

Inlet conditions are as follows. (1) When methane-air equivalence ratio changes, inlet velocity $V = 30$ m/s, and inlet temperature $T = 300$ K. (2) When inlet velocity changes, inlet temperature $T = 300$ K, and methane-air equivalence ratio $\Phi = 0.6$. (3) When inlet temperature changes, inlet velocity $V = 30$ m/s, and methane-air equivalence ratio $\Phi = 0.6$. Details of calculation conditions are listed in Table 2.

3.4.1. The Influence of Equivalence Ratio Φ on the Combustion Flow in TVC. Total pressure loss and combustion efficiency under different equivalence ratios are shown in Figures 13 and 14. The temperature distribution and flow field under different equivalence ratios are shown in Figures 15 and 16.

As can be seen from Figure 13, with the increase of equivalence ratio, total pressure loss increases first and then decreases. When the equivalence ratio is 1, total pressure loss is the largest, about 6.66%. This is because the gas is fully combusted, and the heat release is the largest, so the gas viscosity is increased, which reduces total pressure in the flow process. When the equivalence ratio is 0.6, total pressure loss is 5.12%. In combination with Figure 15, methane can be fully combusted because there is enough air, but there is still a lot of low-temperature air not involved in the reaction, so the temperature is lower. When the equivalence ratio is 1, the high temperature range of the combustion chamber is larger than that of other combustion cases, which indicates that the fuel is fully burned and the heat release is greater. When the equivalence ratio is 1.4, due to the lack of air required for combustion, the fuel directly involved in the reaction is limited and the full combustion is inhibited, so the overall temperature is between the appropriate combustion and lean fuel combustion. Under the condition of lean combustion, total pressure loss is small, and the temperature in the cavity can reach about 2000 K, which can meet the requirement of being a stable ignition source.

It can be seen from Figure 14 that when the equivalence ratio is less than or equal to 1, combustion efficiency is as high as 99.8%, while when the equivalence ratio is greater than 1, combustion efficiency decreases dramatically. When the equivalence ratio is 1.4, combustion efficiency is only 74.4%. This is because under the condition of lean fuel, the

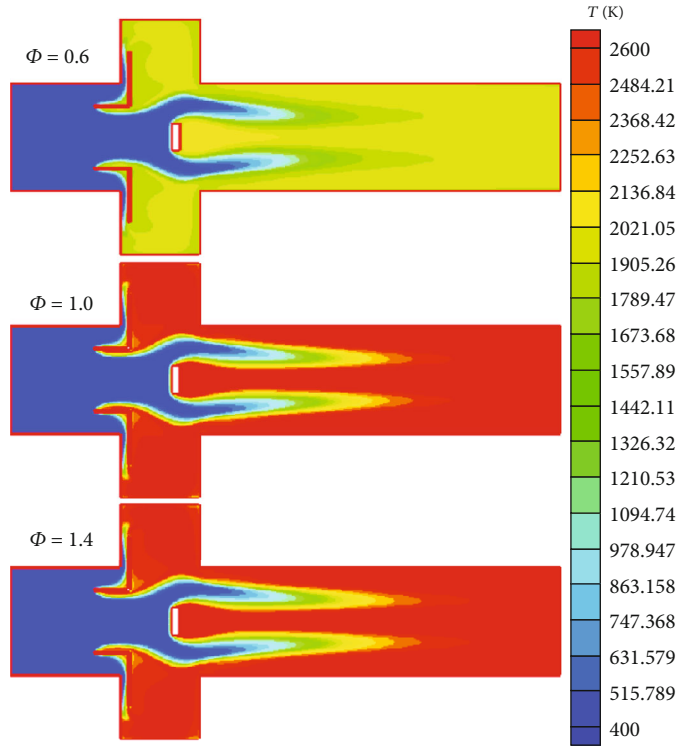

Figure 15: Temperature distribution under different Φ.

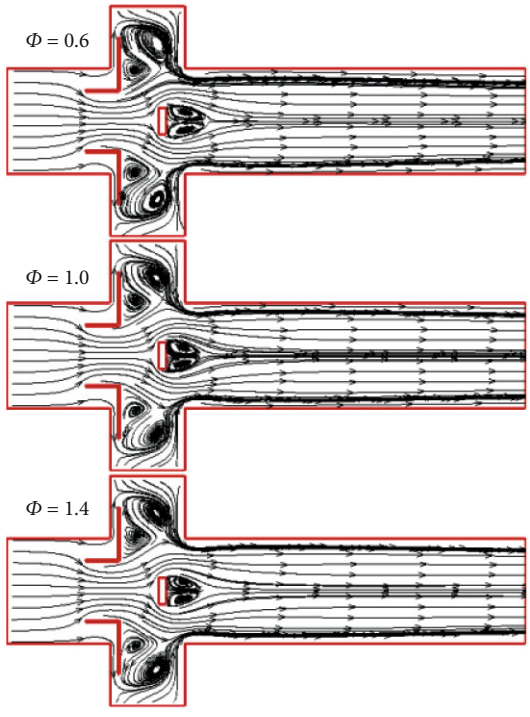

Figure 16: Flow field under different Φ.

sufficient oxygen content makes the fuel fully burn, so combustion efficiency is very high. Under the condition of rich fuel, because the oxygen required for combustion is insufficient, there remains more fuel not fully burned.

The flow field distribution under different equivalence ratios is shown in Figure 16. The flow field distribution is basically the same, the stable double vortex structure can be formed in the cavity, and the shape of the double vortex structure is similar; the secondary vortex core is close to the guide vane, and the main vortex core is in the cavity center, which shows that the influence of different equivalence ratios on the flow field in the cavity is small. In the backflow region behind the blunt body, the vortices are symmetrical along the central section, the vortex structure is similar, but the length is different. With the increase of equivalence ratio, the vortex length decreases.

3.4.2. The Influence of Inlet Velocity V on the Combustion Flow in TVC. Inlet velocity has great influence on total pressure loss. As shown in Figure 17, the increase of inlet velocity makes gas flow more disordered, which results in greater total pressure loss. When inlet velocity is 10 m/s, total pressure loss is the smallest, about 0.62%. When inlet velocity is 50 m/s, total pressure loss is the largest, about 12.36%. However, when inlet velocity is low, the combustion process may be unstable.

From Figure 18, the influence of inlet velocity on combustion efficiency is not obvious. With the increase of inlet velocity, combustion efficiency decreases, but the variation range is very small.

As shown in Figure 19, with the increase of inlet velocity, the temperature increases, especially in the cavity and in the backflow region behind the blunt body. When inlet velocity is 10 m/s, the temperature in the cavity is about 1600 K, and the temperature in the backflow region behind the blunt body is

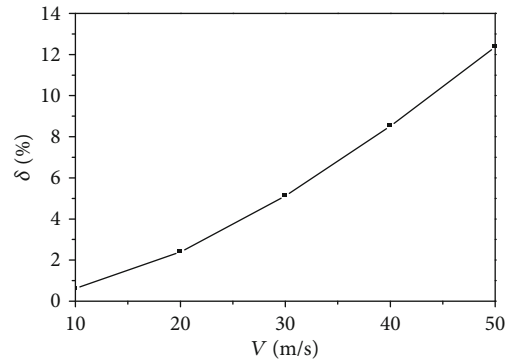

Figure 17: Total pressure loss under different V.

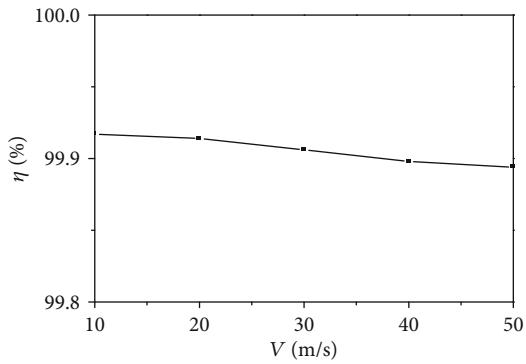

Figure 18: Combustion efficiency under different V.

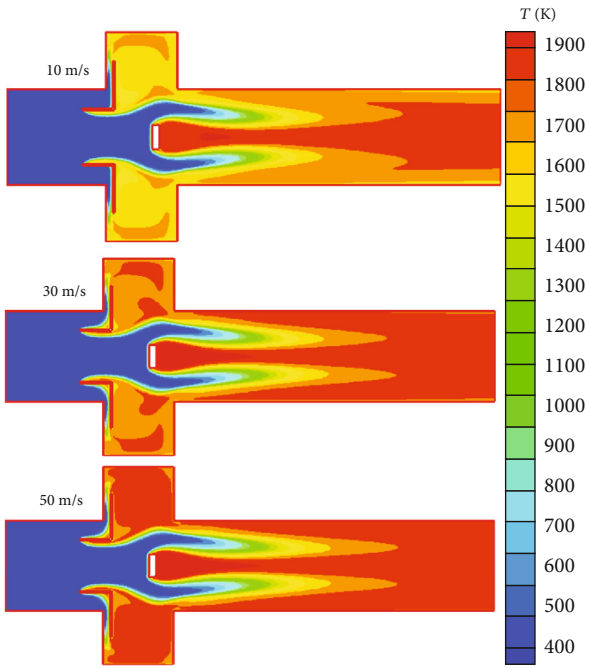

Figure 19: Temperature distribution under different V.

about 1700 K. When inlet velocity is 50 m/s, the temperature in the cavity rises to about 1800 K, and the temperature in the backflow region behind the blunt body is about 1900 K. The

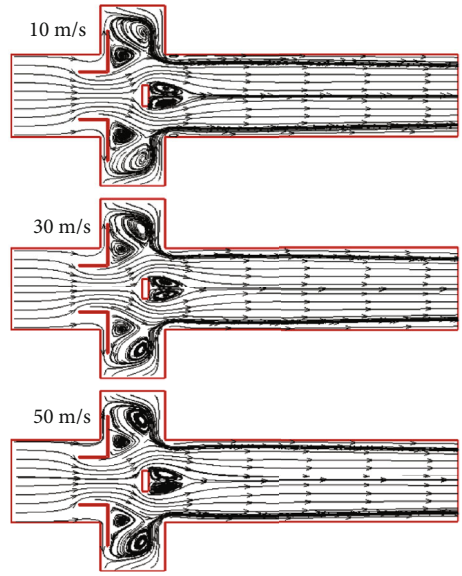

Figure 20: Flow field under different V.

reason is that when inlet velocity is low, the flow velocity in the cavity is too low, the combustion process is unstable, and there are more low-temperature gases entering the cavity, so the temperature is reduced.

From Figure 20, the flow field is basically the same. A symmetrical and stable double vortex structure can be formed in the cavity, and a pair of vortices in the backflow region behind the blunt body is symmetrical along the central section. The secondary vortex exists between the main vortex and the mainstream, which can protect the main vortex and reduce the influence of the mainstream pulsation on the main vortex.

3.4.3. The Influence of Inlet Temperature T on the Combustion Flow in TVC. Figures 21 and 22 show total pressure loss and combustion efficiency distribution under different inlet temperatures.

It can be seen from Figure 21 that total pressure loss decreases with the increase of inlet temperature. When inlet temperature is 300 K, total pressure loss is the largest, about 5.12%. When inlet temperature is 700 K, total pressure loss is the smallest, about 1.44%. This is due to the existence of thermal resistance; the greater the temperature rise, the greater total pressure loss. From Figure 22, combustion efficiency varies little. Figure 23 shows the temperature distribution under different inlet temperatures. With the increase of inlet temperature, the overall temperature of combustor increases, but its temperature rise decreases. When inlet temperature is 300 K, the temperature rise is about 1600 K, while when inlet temperature is 700 K, the temperature rise is about 1400 K, so total pressure loss will be reduced.

Figure 24 shows the flow field under different inlet temperatures. The flow field in the cavity is basically the same, and the stable double vortex structure can be formed in the cavity. Combined with the above analysis, under different inlet temperatures, the flow field in the cavity is maintained in the same state, which shows that the double vortex

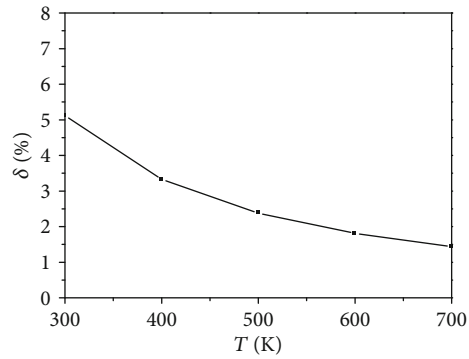

Figure 21: Total pressure loss under different T.

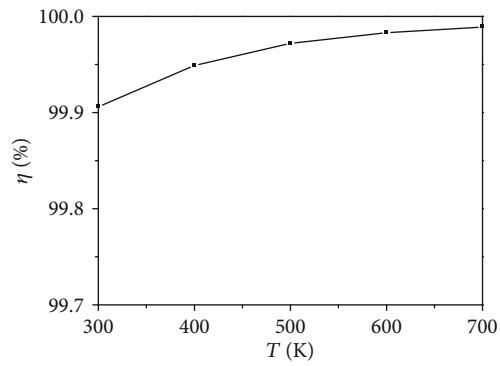

Figure 22: Combustion efficiency under different T.

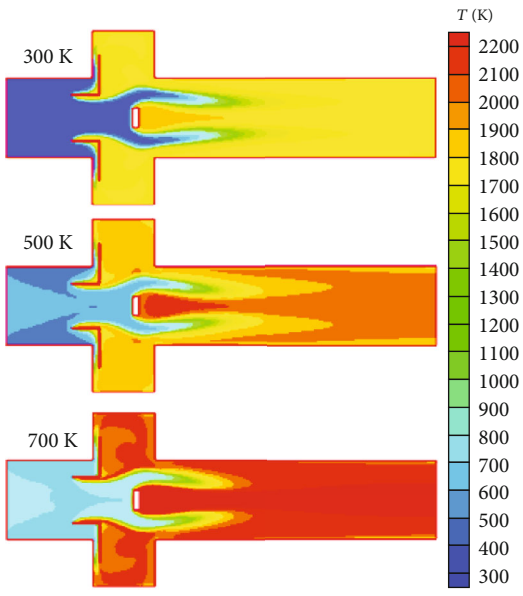

Figure 23: Temperature distribution under different T.

structure in the cavity is very stable. And in the backflow region behind the blunt body, a pair of vortex symmetrical along the central section is formed, but the length of vortex is different. With the increase of inlet temperature, the length of vortex increases.

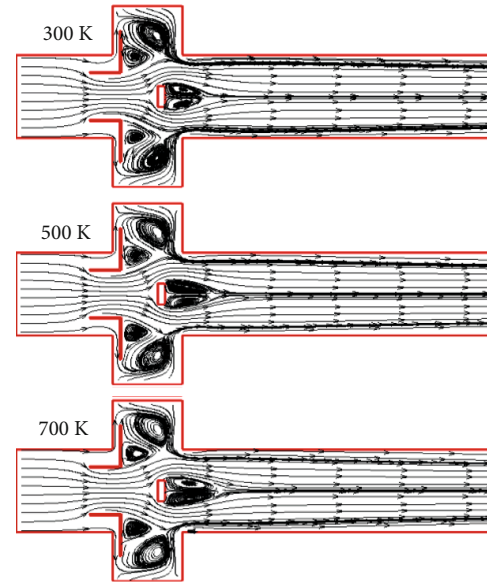

Figure 24: Flow field under different T.

4. Conclusions

Numerical simulation is carried out for TVC with different guide vanes and blunt bodies; the flow field and combustion performance are analyzed. The structure optimization of the combustion chamber is carried out.

(1) The optical blunt body structure is $S/L = 0.7$, $L2/L = 0.1$, and $L1/L_i = 0.25$, and the optical guide vane structure is $a/H_f = 0.5$, $b/L_i = 0.2$, and $c/L = 0.1$. The stable double vortex structure is formed in the cavity, and the better backflow region behind the blunt body is also formed

(2) Double vortices undergo the process of preliminarily forming-breaking down-forming again-being stable gradually. When the mainstream passes over the blunt body, the accelerated mainstream can increase the extrusion on the second vortex and make it relatively more stable

(3) High inlet temperature and low inlet velocity can effectively reduce total pressure loss; equivalence ratio has little effect on total pressure loss. The combustion chamber works better in lean condition, and the influence of inlet temperature and inlet velocity on combustion efficiency is small

Data Availability

The data of this study is available from Capacity Building Projects in Local Universities of Science and Technology Commission of Shanghai Municipality (19020500900).

Conflicts of Interest

The authors declare that there is no conflict of interest regarding the publication of this paper.

Acknowledgments

This work was financially supported by Capacity Building Projects in Local Universities of Science and Technology Commission of Shanghai Municipality (19020500900).

References

[1] K. Hsu, L. Gross, D. Trump, and W. Roquemore, "Performance of a trapped-vortex combustor," in *33rd Aerospace Sciences Meeting and Exhibit*, Reno,NV,U.S.A., 1995.

[2] K. Zbeeb, "Fuel injector Reynolds number effects on performance and emissions of a trapped vortex combustor," in *23rd AIAA Computational Fluid Dynamics Conference*, Denver, CO, United states, 2017.

[3] Z. Fu, H. Gao, Z. Zeng, J. Liu, and Q. Zhu, "Generation characteristics of thermal NO_x in a double-swirler annular combustor under various inlet conditions," *Energy*, vol. 200, article 117487, 2020.

[4] P. Jiang and X. M. He, "Ignition characteristics of a novel mixed-flow trapped vortex combustor for turboshaft engine," *Fuel*, vol. 261, article 116430, 2020.

[5] Z. Zeng, H. Cheng, and Z. Wang, "Investigation of the flow and heat transfer characteristics in advanced vortex combustor," *International Journal of Thermal Sciences*, vol. 156, article 106459, 2020.

[6] P. K. E. Kumar and D. P. Mishra, "Numerical study of reacting flow characteristics of a 2D twin cavity trapped vortex combustor," *Combustion Theory and Modelling*, vol. 21, no. 4, pp. 658–676, 2017.

[7] S. Chen and D. Zhao, "Numerical study of guide vane effects on reacting flow characteristics in a trapped vortex combustor," *Combustion Science and Technology*, vol. 190, no. 12, pp. 2111–2133, 2018.

[8] Y. Zhu, Y. Jin, and X. He, "Effects of location and angle of primary injection on the cavity flow structure of a trapped vortex combustor model," *Optik*, vol. 180, pp. 699–712, 2019.

[9] M. Li, X. He, Y. Zhao, Y. Jin, Z. Ge, and W. Huang, "Effect of strut length on combustion performance of a trapped vortex combustor," *Aerospace Science and Technology*, vol. 76, pp. 204–216, 2018.

[10] R. Sharifzadeh and A. Afshari, "Numerical investigation of flow field effects on fuel–air mixing in a non-reacting trapped vortex combustor with different injection arrangements," *European Journal of Mechanics-B/Fluids*, vol. 82, pp. 106–122, 2020.

[11] P. K. Ezhil Kumar and D. P. Mishra, "Combustion characteristics of a two-dimensional twin cavity trapped vortex combustor," *Journal of Engineering for Gas Turbines and Power*, vol. 139, no. 7, article 071504, 2017.

[12] Z. Wu and X. He, "Investigations on emission characteristics of a liquid-fueled trapped vortex combustor," *Journal of Thermal Science*, vol. 29, no. 1, pp. 69–80, 2020.

[13] J. Xie and Y. Zhu, "Characteristics study on a modified advanced vortex combustor," *Energy*, vol. 193, article 116805, 2020.

[14] Y. Deng, L. Zheng, F. Su, and C. Ma, "Flow and combustion characteristics of annular advanced vortex combustor," in *Proceedings of the ASME 2016 International Mechanical Engineering Congress and Exposition*, vol. 6A, Phoenix, AZ, United states, 2016.

[15] Z. Zeng, P. Du, Z. Wang, and K. Li, "Combustion flow in different advanced vortex combustors with/without vortex generator," *Aerospace Science and Technology*, vol. 86, pp. 640–649, 2019.

[16] K. K. Agarwal, S. Krishna, and R. V. Ravikrishna, "Mixing enhancement in a compact trapped vortex combustor," *Combustion Science and Technology*, vol. 185, no. 3, pp. 363–378, 2013.

[17] K. K. Agarwal and R. V. Ravikrishna, "Experimental and numerical studies in a compact trapped vortex combustor: stability assessment and augmentation," *Combustion Science and Technology*, vol. 183, no. 12, pp. 1308–1327, 2011.

[18] T. H. Shih, W. W. Liou, A. Shabbir, Z. Yang, and J. Zhu, "A new k-ϵ eddy viscosity model for high Reynolds number turbulent flows," *Computers fluids*, vol. 24, no. 3, pp. 227–238, 1995.

[19] B. F. Magnussen and B. H. Hjertager, "On mathematical models of turbulent combustion with special emphasis on soot formation and combustion," in *Symposium (international) on Combustion*, vol. 16, no. 1pp. 719–729, The Combustion Institute, 1977.

[20] D. B. Spalding, "Numerical computation of multiphase fluid flow and heat transfer," in *Recent Advances in Numerical Methods in Fluids*, vol. 1, pp. 139–167, Pineridge Press Limited, Swansea, UK, 1980.